14. COIL MECHANICAL ANALYSES

In this chapter we will summarise the main results of the 2-D axisymmetric mechanical analyses carried out to date on the CMS coil. A quick outline of on going and future activities will also be given [14-1].

The coil has been simulated at two of its operating conditions:
- Coil at 4.5 K.
- Coil energised (4.5 K, 19.5 kA, 4.05 T).

Several simulations have been carried out for different conductor configurations [14-2], [14-3]. The results presented in this chapter are those obtained for the block conductor (see Fig. 12.1).

The analyses have been carried out in parallel at INFN-Genova and CEA-Saclay using two different FE codes (ANSYS and CASTEM respectively) [14-4].

The results of the analyses for the previous CMS coil configurations as well as for the windings with different conductors can be found in several technical notes issued both by INFN and CEA-Saclay [14-5], [14-6], [14-7], [14-8], [14-9], [14-10], [14-11].

14.1 MAGNETIC FEA

14.1.1 The magnetic FE model

A magnetic FEA was performed to calculate the Lorenz force distribution to be used in the stress FEA. The calculation is non linear due to the B-H curve of the iron. More detailed magnetic computations are reported in Chapt. 6.

The geometry of the iron yoke used in the magnetic analysis is shown in Fig. 14.1. The following approximations have been made in the model:
- the dodecagonal prisms of the barrel and the end-cap are transformed into cylinders of the same cross sectional area,
- the hole of the chimney in the barrel has been neglected,
- the current (19.5 kA) in the winding has been modelled as uniformly distributed in 4 shells of the same radial thickness of the Rutherford cable.

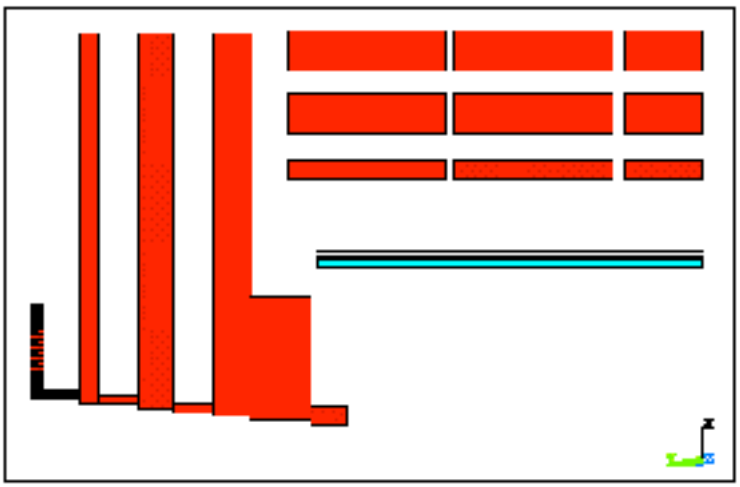

Fig. 14.1: Iron yoke geometry used in the magnetic FEA.

14.1.2 Magnetic FEA results

The B field contour plot and the integral axial force as a function of z are shown in Fig. 14.8, p. C-39 and Fig. 14.2.

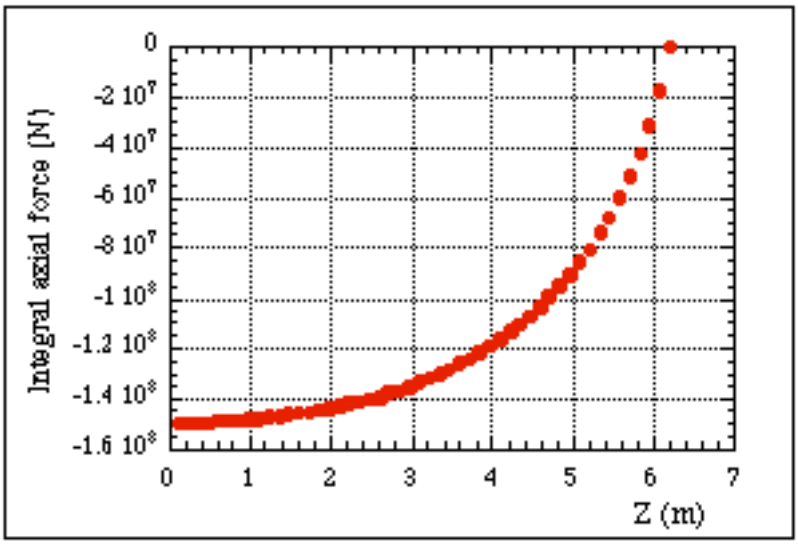

Fig. 14.2: Integral axial force as a function of Z.

14.2 STRESS FEA

14.2.1 Material properties

The behaviour of the different materials has been modelled as follows:

- Electrical insulation: elastic and orthotropic material.
- Aluminium alloy: elastic and isotropic material.
- Pure aluminium: elasto-plastic isotropic material with kinematic hardening rule.

The experimental stress strain curves measured at 4.2 K are shown in Fig. 14.3 for annealed and cold worked Al (after 4-5 energisation cycles) [14-12].

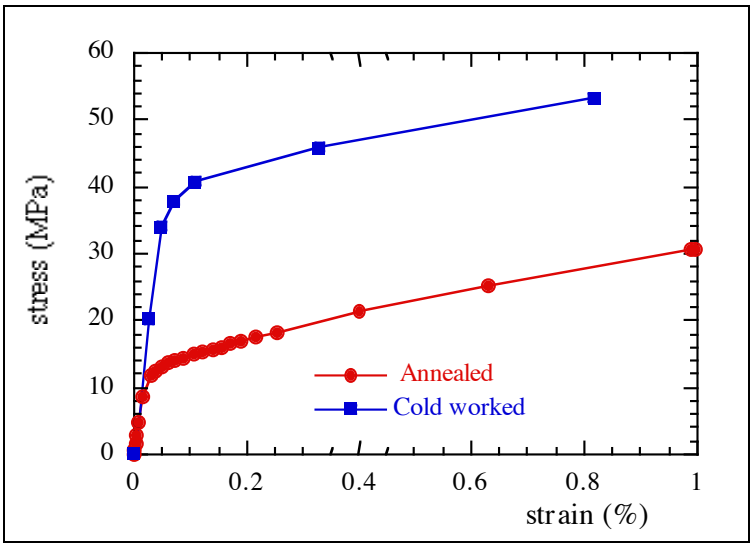

Fig. 14.3: Experimental stress strain curves, measured at 4.2 K, of pure Al both fully annealed

and cold worked after 4-5 energisation cycles.

Table 14.1
Material properties used in the FEA.

Material	Temperature K	Young's Modulus GPa	Poisson's ratio
Al	4.2	see Fig. 14.3	0.49
Al-alloy	4.2	77.7	0.327
Sc strand	4.2	130	0.3
Fibre glass epoxy // to fibre direction	4.2	20	0.21
Fibre glass epoxy ^ to fibre direction	4.2	12.5	0.21

Table 14.2
Mean integral thermal expansion coefficients used in the FEA.

Material	Mean integral thermal expansion coefficient 293 K - 4.2 K K^{-1}
Aluminium	$14.23\ 10^{-6}$
Al-alloy	$14.16\ 10^{-6}$
Sc strand	$8.79\ 10^{-6}$
Fibre glass epoxy // to fibre	$8.45\ 10^{-6}$
Fibre glass epoxy ^ to fibre	$25.5\ 10^{-6}$

14.2.2 The mechanical FE model

The coil has been simulated with an elasto-plastic 2-D axisymmetric FE model. A sub-modelling technique had to be used for the FEA due to the size of the problem and its non linearity, which comes in with the plastic flow of pure aluminium. Two locations: coil end and coil centre were chosen for the sub-modelling. Each sub-modelling location comprises 4 layers and 8 turns.

Several sub-models (see Fig. 14.4 and Fig. 14.5) for different locations and different degrees of detail have been run. No major differences were found between the stress distribution of the aligned turn and the staggered turn winding configuration. The results presented here are those of the sub-model with aligned turns.

As already mentioned at the beginning of the chapter, the stress analyses have been carried out for two main operating conditions:

- Coil at 4.5 K.
- Coil at 4.5 K energised.

The real load history of the coil should in principle have been taken into account in our modelling, as the problem is non conservative (i.e. history dependent) due to the plastic flow of pure Al. However, for these analyses, one single load step both for cool-down and

energisation has been used. This is a fair approximation if one assumes monotonic cooling and energisation.

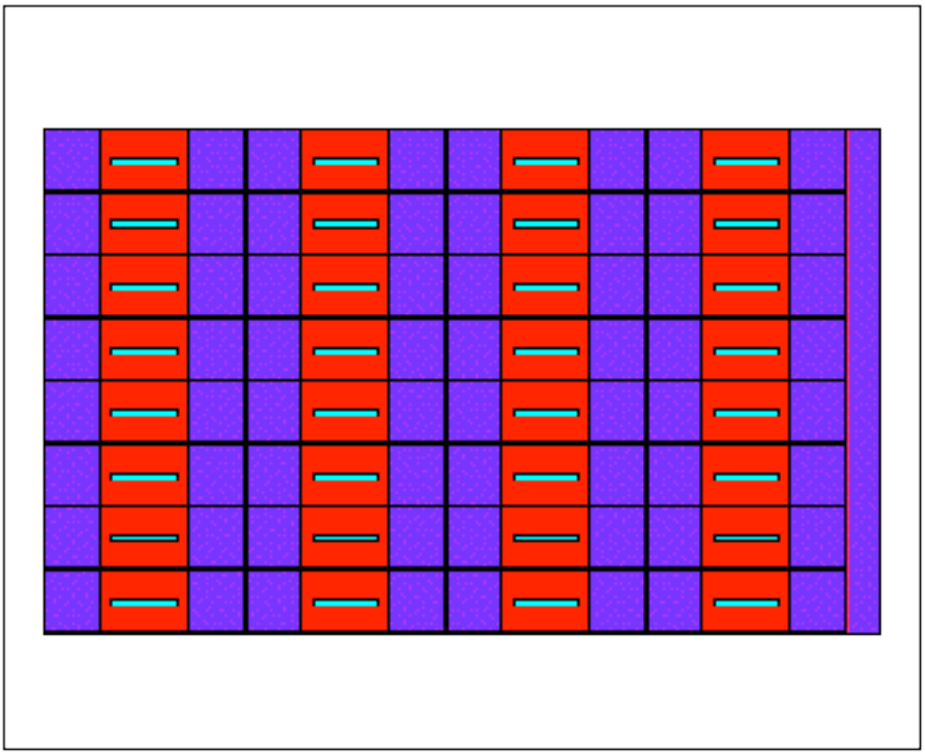

Fig. 14.4: Sub-model with aligned turns.

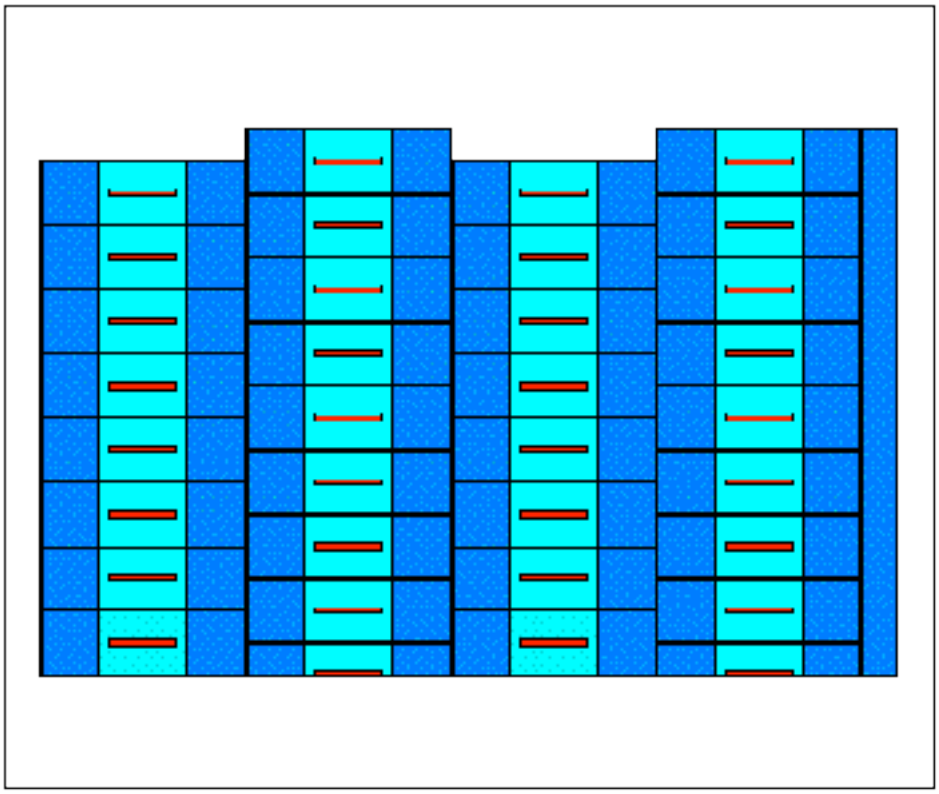

Fig. 14.5: Sub-model with staggered turns.

14.2.3 Stress FEA results

Analyses criteria

The Von Mises criterion has been used for all ductile materials present in the winding.

For the insulation, which behaves in an elasto-brittle way, a criterion which takes into account the hydrostatic component of the stress tensor must be used. In our case the Mohr-Coulomb criterion has been adopted. According to this criterion the calculated distribution of points (s_{mean}, t_{max}) must lay within an experimental failure envelope. If the material is isotropic the implementation of Mohr-Coulomb is straightforward. In the case of an anisotropic material, on the other hand, the use of this criterion is not trivial due to the fact that the envelope is not univocal. One way around this problem is to consider the most restrictive envelope. However, since the scatter of the failure envelopes in terms of stress is greater than those in terms of strain, a strain based Mohr-Coulomb criterion should be used [14-4], [14-13]. In order to do so the experimental strain failure envelope is needed. At present, the only experimental information available is relative to stress envelopes. So, even if not ideal, the results of the analyses are presented here in terms of stress.

For the interfaces the results were extracted from the FEA in a form which could be compared with the experimental data available.

Stresses in the conductor

The pure aluminium has been modelled with annealed state properties. This has been done in order to calculate the maximum strains seen by the winding throughout its working life. The stress values obtained in this analysis are obviously lower than those obtained with a cold worked aluminium. When comparing FEA with experimental results one must bear in mind the Al properties used in the modelling.

A summary of the results is given in Tables 14.3, 14.4 and 14.5. The maximum stress levels are shown together with the location.

Table 14.3
Maximum Von Mises stress in conductor's components.

Material	Von Mises stress, MPa Coil End	Von Mises stress, MPa Coil centre
Coil at 4.5 K		
Pure Aluminium	2 - 21	4 - 21
SC Cable	200 - 246	200 - 246
Al alloy	0 - 62	0 - 62
Coil at 4.5 K, energised		
Pure Aluminium	9 - 23	9 - 25
SC Cable	80 - 191	38 - 200
Al alloy	62 - 100	112 - 139

In the loadcase of the Coil at 4.5 K the maximum Von Mises values found in the pure Al are in fact stress concentrations localised around the Rutherford cable.

Peak Von Mises stresses only increase by few MPa's when the magnet is energised. However, it must be noted that, in this loadcase, high Von Mises stress values appear all over

the cross section of the Al-stabiliser.

Stress contour plots of the different details of the winding are shown in Figs 14.9 and 14.10, p. C-40 to Figs 14.11 and 14.12, p. C-41.

Table 14.4
Maximum Von Mises and Shear stresses at interfaces (Al side): Coil end.

Material Bonding	Max Von Mises stress MPa	Max Shear stress MPa
Coil at 4.5 K		
SC Cable ÷ Pure Aluminium	15 - 21	12
Pure Aluminium ÷ Al Alloy	7 - 17	10
Coil at 4.5 K, energised		
SC Cable ÷ Pure Aluminium	13 - 23	13
Pure Aluminium ÷ Al Alloy	12 - 19	10

Table 14.5
Maximum Von Mises and Shear stresses at interfaces (Al side): Coil centre.

Material Bonding	Max Von Mises stress MPa	Max Shear stress MPa
Coil at 4.5 K		
SC Cable ÷ Pure Aluminium	15 - 21	12
Pure Aluminium ÷ Al Alloy	7 - 17	10
Coil at 4.5 K, energised		
SC Cable ÷ Pure Aluminium	14 - 24	13
Pure Aluminium ÷ Al Alloy	11 - 19	10

Stresses in the insulation

Maximum and minimum values of shear at the interface are given in Tables 14.6 and 14.7. The (s_{mean}, t_{max}) distributions shown in Fig. 14.6 and Fig 14.7 fall well within the failure envelopes found in the literature [14-14].

Table 14.6
Maximum values of shear stress at insulation–conductor interface.

Coil at 4.5 K	Shear stress MPa
Coil end location	10
Coil centre location	10

Table 14.7
Maximum values of shear stress at insulation–conductor interface.

Coil at 4.5 K, energised	Shear stress MPa

Coil end location	10
Coil centre location	10

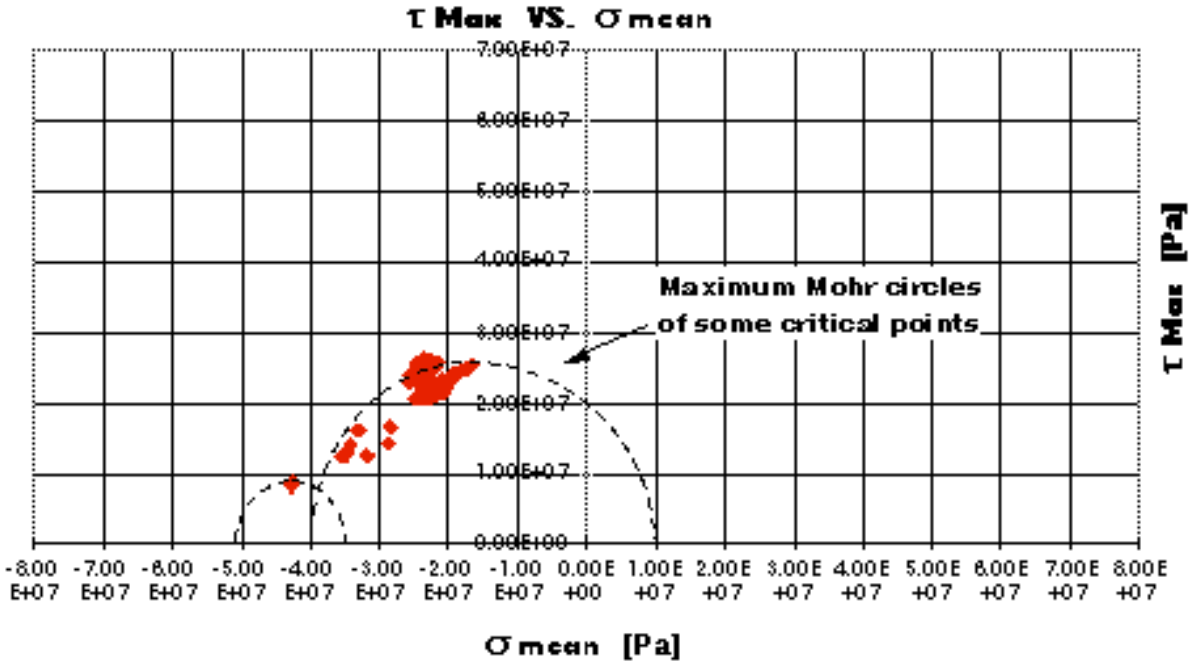

Fig. 14.6: Coil centre location - Coil at 4.5 K: (s_{mean}, t_{max}) distribution in the insulation.

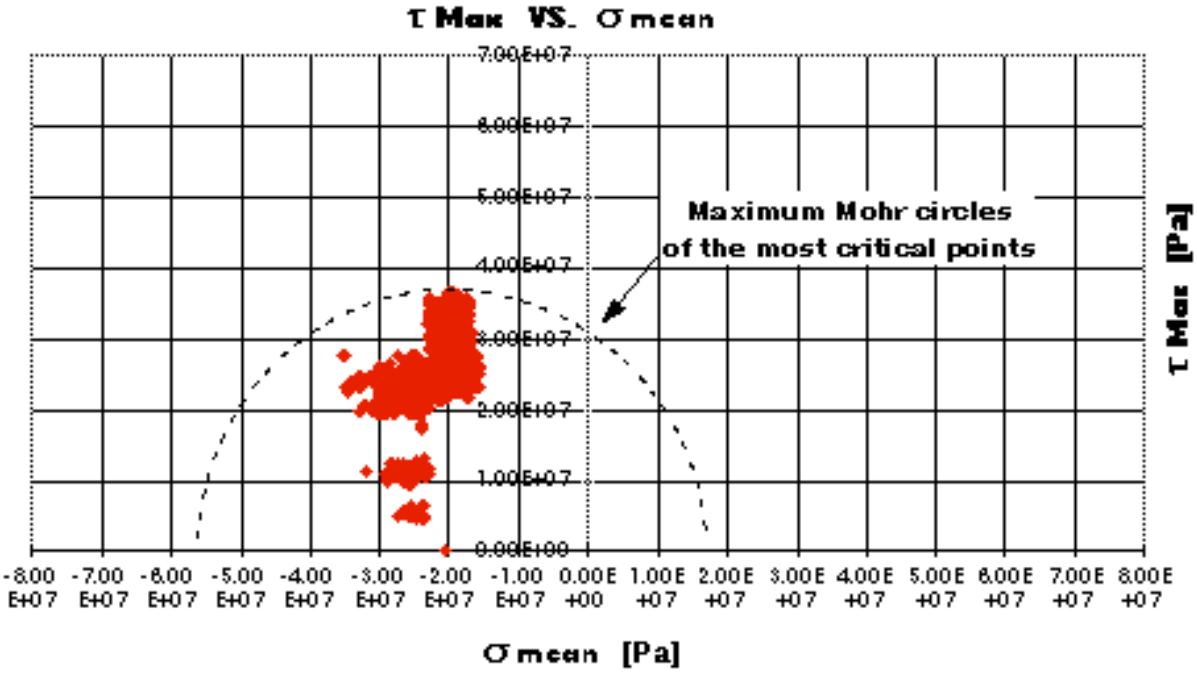

Fig. 14.7: Coil centre location - Coil at 4.5 K, 4T: (s_{mean}, t_{max}) distribution in the insulation.

14.3 CONCLUSIONS

Insulation

Cool down gives the largest contribution to the stress field in the insulation, on the other hand the effect of the EM forces seems to be relatively small.

Some analysis is under way to investigate the influence of the winding helix on the stress field in the insulation. Another important outstanding issue is the effect of the conductor corner fillet.

On the experimental side a set of samples is being designed, at CERN and CEA, Saclay, in order to validate a Mohr-Coulomb strain based failure criterion to be used in our future FEA's. Other tests to study the failure mechanism at the interface are also being considered.

Aluminium

The pure Al stabiliser is well into the plastic domain. The present conductor geometry has been chosen to minimise most of the structural function of the pure Al. Tests have been planned at CERN and ETH on several issues regarding the Rutherford/Al interface [14-15].